

Modified constraint-induced movement therapy alters synaptic plasticity of rat contralateral hippocampus following middle cerebral artery occlusion

Bei-Yao Gao¹, Dong-Sheng Xu^{2,3}, Pei-Le Liu¹, Ce Li¹, Liang Du¹, Yan Hua¹, Jian Hu¹, Jia-Yun Hou⁴, Yu-Long Bai^{1,*}

¹ Department of Rehabilitation Medicine, Huashan Hospital, Fudan University, Shanghai, China

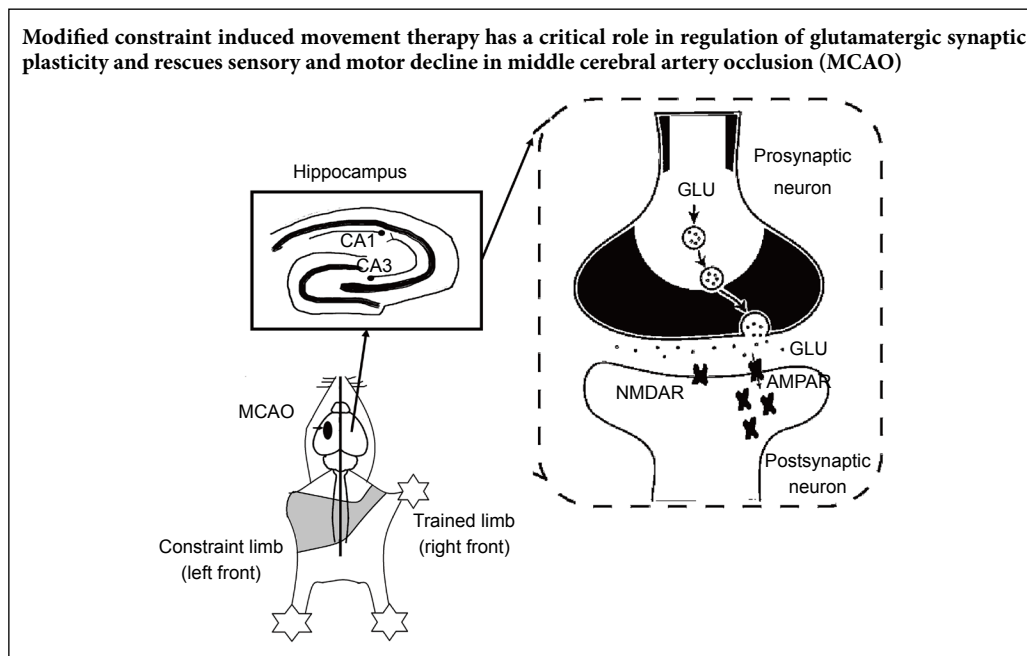
² Rehabilitation Section, Department of Spine Surgery, Tongji Hospital of Tongji University, Shanghai, China

³ Key Laboratory of Spine and Spinal Cord Injury Repair and Regeneration (Tongji University) Ministry of Education, Shanghai, China

⁴ Zhongshan Hospital Institute of Clinical Science, Fudan University, Shanghai, China

Funding: The study was supported by the National Natural Science Foundation of China, No. 81871841 (to YLB) and No. 81772453 (to DSX).

Graphical Abstract



*Correspondence to:
Yu-Long Bai, MD, PhD,
dr_baiyl@fudan.edu.cn.

orcid:
0000-0003-0461-1506
(Yu-Long Bai)

doi: 10.4103/1673-5374.270312

Received: June 27, 2019
Peer review started: July 4, 2019
Accepted: August 12, 2019
Published online: December 10, 2019

Abstract

Modified constraint-induced movement therapy is an effective treatment for neurological and motor impairments in patients with stroke by increasing the use of their affected limb and limiting the contralateral limb. However, the molecular mechanism underlying its efficacy remains unclear. In this study, a middle cerebral artery occlusion (MCAO) rat model was produced by the suture method. Rats received modified constraint-induced movement therapy 1 hour a day for 14 consecutive days, starting from the 7th day after middle cerebral artery occlusion. Day 1 of treatment lasted for 10 minutes at 2 r/min, day 2 for 20 minutes at 2 r/min, and from day 3 onward for 20 minutes at 4 r/min. CatWalk gait analysis, adhesive removal test, and Y-maze test were used to investigate motor function, sensory function as well as cognitive function in rodent animals from the 1st day before MCAO to the 21st day after MCAO. On the 21st day after MCAO, the neurotransmitter receptor-related genes from both contralateral and ipsilateral hippocampi were tested by micro-array and then verified by western blot assay. The glutamate related receptor was shown by transmission electron microscopy and the glutamate content was determined by high-performance liquid chromatography. The results of behavior tests showed that modified constraint-induced movement therapy promoted motor and sensory functional recovery in the middle cerebral artery-occluded rats, but had no effect on cognitive function. The modified constraint-induced movement therapy upregulated the expression of glutamate ionotropic receptor AMPA type subunit 3 (Gria3) in the hippocampus and downregulated the expression of the beta3-adrenergic receptor gene *Adrb3* and arginine vasopressin receptor 1A, *Avpr1a* in the middle cerebral artery-occluded rats. In the ipsilateral hippocampus, only *Adra2a* was downregulated, and there was no significant change in *Gria3*. Transmission electron microscopy revealed a denser distribution the more distribution of postsynaptic glutamate receptor 2/3, which is an α -amino-3-hydroxy-5-methyl-4-isoxazole-propionic acid receptor, within 240 nm of the postsynaptic density in the contralateral cornu ammonis 3 region. The size and distribution of the synaptic vesicles within 100 nm of the presynaptic active zone were unchanged. Western blot analysis showed that modified constraint-induced movement therapy also increased the expression of glutamate receptor 2/3 and brain-derived neurotrophic factor in the hippocampus of rats with middle cerebral artery occlusion, but had no effect on Synapsin I levels. Besides, we also found modified constraint-induced movement therapy effectively reduced glutamate content in the contralateral hippocampus. This study demonstrated that modified constraint-induced movement therapy is an effective rehabilitation therapy

in middle cerebral artery-occluded rats, and suggests that these positive effects occur via the upregulation of the postsynaptic membrane α -amino-3-hydroxy-5-methyl-4-isoxazole-propionic acid receptor expression. This study was approved by the Institutional Animal Care and Use Committee of Fudan University, China (approval No. 201802173S) on March 3, 2018.

Key Words: brain-derived neurotrophic factor; glutamate; hippocampus; mCIMT; middle cerebral artery occlusion; modified constraint-induced movement therapy; α -amino-3-hydroxy-5-methyl-4-isoxazole-propionic acid receptor

Chinese Library Classification No. R455; R741; G804.55

Introduction

Stroke is characterized by high disability, high mortality, and a high recurrence rate, and is the most common cause of death worldwide (Langhorne et al., 2018). Disability caused by stroke can directly lead to job loss, which places a heavy burden on patients, their families, and society – about 40% of stroke survivors experience some kind of disability (Feigin et al., 2016). Constraint-induced movement therapy (CIMT) is an intensive rehabilitation treatment that promotes use of the unaffected side by limiting the unaffected side. However, the treatment can cause discomfort and emotional anxiety during daily activities because patients are required to wear an auxiliary device, like a sling or splint or gloves for 90% of their waking time (Park et al., 2015; Liu et al., 2019; Zhai and Feng, 2019). To minimize these limitations, modified CIMT (mCIMT) has been designed, and the main difference between the two forms is the duration of mandatory training and the time limit for using the unaffected hand (Kwakkel et al., 2015). Several randomized control trials have shown that mCIMT is a feasible and potentially effective tool after stroke (Baldwin et al., 2018; Bang et al., 2018). However, the mechanism underlying the improvement following mCIMT is not yet fully understood, and comprehensive behavioral assessments in animals are also lacking.

In both adult and pediatric CIMT studies, increases in hippocampal activity have been observed using functional magnetic resonance imaging (Gauthier et al., 2008; Sterling et al., 2013). Although most studies on motor control have focused on the primary motor cortex, motor control also involved the hippocampus, which also has a unique contribution to memory (Kerr et al., 2017). Therefore, the present mechanistic study was confined to the hippocampus. Previous findings have reported that physical exercise has beneficial effects on hippocampal spinogenesis, neurogenesis, and synaptic plasticity (van Praag et al., 1999; Stranahan et al., 2007; Dietrich et al., 2008; Yau et al., 2011, 2014). One study has indicated that the number of new dendrites and newborn granule cells remained unchanged in animals that underwent CIMT (Qu et al., 2015), which suggests that plastic changes may instead occur in mature neurons. Furthermore, synaptic plasticity has been shown to be one of the neurobiological bases for functional recovery after stroke (Coleman et al., 2017; Sandvig et al., 2018). Pathophysiological development process in animal models of stroke showed that middle cerebral artery occlusion (MCAO) as remote sensorimotor stroke modifies the activity of hippocampal-thalamic networks (Bast and Feldon, 2003; Baumgartner et al., 2018). Exercise training alleviates sensorimotor deficits and improves motor function

following ischemia (Kerr et al., 2017; Nie and Yang, 2017).

The α -amino-3-hydroxy-5-methyl-4-isoxazolepropionic acid receptor (AMPA), one of the most important neurotransmitter receptors, is activated by binding to glutamate. The AMPAR subunits glutamate receptor GluR2 and GluR3 play a crucial role in helping the excitatory postsynaptic current (EPSC) amplitude flow through AMPA channels, and the GluR2 subunit can also be selectively altered during synaptic plasticity, as well as during cerebral ischemia/reperfusion injury (Isaac et al., 2007; Chen and Wang, 2016; Takemoto et al., 2017). Furthermore, the effects of rehabilitative training are affected by changes in postsynaptic membrane AMPAR expression. Researchers have found that motor skills training enhanced the expression level of AMPAR mRNA in the sensorimotor cortex and striatum after brain damage (Tamakoshi et al., 2017). However, the effects of mCIMT on AMPAR during the stroke recovery process are unclear. Glutamate, which is the main excitatory neurotransmitter, is involved in the regulation of a variety of physiological functions, such as learning, memory, cognition, mood, and exercise (Vandenberg and Ryan, 2013). Previous studies have demonstrated that CIMT increased the levels of synaptic neurotransmitter regulation, and improved behavior sensorimotor and cognitive outcomes (Zhao et al., 2013). However, the effects of the potentiation of synaptic transmission that occurs during CIMT have not yet been fully elucidated. Therefore, it is essential to measure AMPAR and glutamate content and distribution; furthermore, changes in synapse activation need to be measured using morphological methods.

In this study, we explored mCIMT-induced behavioral changes, and also analyzed the ability of mCIMT to induce hippocampus plasticity, modify brain microscopic morphology, and form more synaptic transmissions in a left MCAO rat model. Here, we used the immune colloidal gold technique to identify the molecular and metabolic mechanisms at the synaptic level.

Materials and Methods

Animals

Eighteen male Sprague-Dawley rats, weighing 250–300 g and aged 7–9 weeks, were provided by Shanghai SIPPR-BK LAB Animal Ltd., Shanghai, China (license No. SCXK (Hu) 2013-0016). The rats were housed in clean grade animal facilities in groups of 4, with a 12-hour light/dark cycle (lights off at 8 p.m.) and free access to food and water. The experimenters were blinded to all experimental conditions until all data were obtained. Unless otherwise specified, the rats were randomly assigned to different groups in all experiments. The

rats were randomly allocated to the sham group (sham; $n = 6$); MCAO group (MCAO; $n = 6$), or mCIMT group (MCAO + mCIMT; $n = 6$). All experiments were approved by the Institutional Animal Care and Use Committee of Fudan University, China (approval No. 201802173S) on March 3, 2018.

Transient MCAO model

Transient MCAO was performed as described previously (Liang et al., 2018). Briefly, rats were anesthetized using 10% chloral hydrate, and the rectal temperature was monitored and kept at around 36.5°C. Ischemia was induced by inserting a poly-L-lysine-coated filament into the left middle cerebral artery (Beijing Cinontech Co. Ltd., Beijing, China). After 90 minutes, the filament was retracted. Blood flow was monitored by laser Doppler anemometry (Moor Instruments Ltd., Millwey, UK). Cerebral blood flow was monitored during the entire surgical procedure, including the period before, during, and after MCAO. Rats in the sham group underwent the MCAO procedures without insertion of the filament and occlusion of the middle cerebral artery. Neurologic deficits were measured with neurological 0–4 level scores post anesthesia (Longa et al., 1989). Rats with score of 0 or 4 were excluded from the study.

mCIMT

In mCIMT, a flexible bandage was used to tie the unaffected limb, the left forelimb, to the chest and fix it for 2 hours per day. mCIMT was started for two weeks on the 7th day after MCAO. Day 1 of treatment lasted for 10 minutes at 2 r/min, day 2 for 20 minutes at 2 r/min, and from day 3 onward for 20 minutes at 4 r/min. The training time for walking inside the wheel equipment was 1 hour per day. Training ended during Suspend training during the behavioral test period. Before the first training, the rats were familiarized with the treadmill (China patent No. 201008862247.8) for 20 minutes.

Gait analysis

The video-based digital gait analysis system CatWalk 7.1 unit (Noldus Information Technology, Wageningen, Netherlands) consisted of a 130-cm glass runway that was parallel to the internal components of its internal lighting. For each rat, recordings were only included when all four paws should complete at least three passage through the glass runway, while the camera recorded these paw prints. CatWalk[®] 7.1 software (Noldus Information Technology) was applied to analyze gait-related parameters, including the intensity of the complete paw (both right front and right hind paw), which reflected the force exerted by the paw and gait speed (Hu et al., 2019). Before MCAO, the rats had three days of familiarization with the equipment and the apparatus. The day of the MCAO was regarded as day 1, and the day before MCAO was considered as day 0. Each rat was tested on days 0, 7, and 21. The gait analysis experiment was performed by an investigator who was blinded to the group information.

Adhesive removal test

Motion and sensory function was assessed by the adhesive

removal test. Animal cages were placed in the test chamber at least 30 minutes prior to the start of the experiment to allow for adaptation to the new environment. After that, the animals were removed from their home cages and placed in the laboratory for a 60-second acclimation period. The adhesive removal test was performed as described previously (Bouet et al., 2009). It consists of applying adhesive tape on each forepaw of the rats, and collecting the time taken to contact the tape on the affected forepaw and the time to remove the tape. The day before MCAO was referred to day 0, and each rat was tested on days 0, 6, 9, 15, and 20. The test was performed by the same investigator who was blinded to the group allocation.

Y-maze test

Learning and memory function was assessed using the Y maze. Each rat was placed at the end of one arm and allowed to pass freely through the maze (RD1102-YM-rat; Shanghai Shift Mobeidatum Co., Ltd., Shanghai, China) for 8 minutes. The Y-maze test was performed as described previously (Kraeuter et al., 2019). Each arm of the labyrinth was 40 cm long, and the angle between the three arms was 120°. An alternation was defined as entries into all three arms consecutively without repetition. The maximum number of alternations was calculated as the total number of times entering all arms minus two. The alternating percentage was (collected alternations/maximum alternations) \times 100%. Each rat was tested on days 0, 7, 14, and 21. The analysis was performed by an investigator who was blinded to the group information.

Real-time quantitative PCR and microarray

Rats were sacrificed under anesthesia on day 21 after MCAO established. Approximately 1 mL Trizol was used for one brain sample, which was fully lysed at room temperature for 5 minutes. Chloroform (200 μ L) and isopropanol (0.5 mL) were used for total RNA extraction. After centrifuging at 12,000 \times g for 15 minutes, we transferred upper aqueous phase, then collected the RNA that had sunk to the bottom of the tube, dried it at room temperature, then dissolved RNA samples with 50 μ L H₂O. RNA concentration and purity were determined using the BIOTEK Epoch UV machine (BioTek Epoch full wavelength microplate reader, BioTek Epoch, Winooski Vermont, VT, USA) and Epoch+Take3 Ultra Micro Board (16 fluxes)(BioTek Epoch, Winooski Vermont, VT, USA). Gel electrophoresis assays were used to identify, quantify, and purify nucleic acid fragments and assess their quality. Reverse transcription reactions were carried out according to the protocol from Takara Bio's reverse transcription kit (PrimeScript[™] RT reagent Kit with gDNA Eraser Item No. RR047A, Takara Shuzo Co., Ltd, Kusatsu, Japan) and quantitative PCR reactions were carried out according to the quantitative PCR Test Kit (GoTaq[®] qPCR Master Mix Item No. A6001, Promega Corporation, Madison, WI, USA). The rat neuroreceptor gene microarray (Wcgene Biotech, Shanghai, China) was used to detect 84 genes of encoding the neurotransmitter receptor system according to the manufacturer's protocol. The collected data were analyzed using

WcGene Biotech software (<http://www.wcGene.com>). The statistical analysis results and genes are listed in **Table 1** and **Additional Table 1**, respectively.

Western blot assay

The hippocampi of rats 21 days after MCAO were dissected in radioimmunoprecipitation assay buffer, and equal amounts of proteins were separated using sodium dodecyl sulfate-polyacrylamide gel electrophoresis. The protein was blotted onto a polyvinylidene difluoride membrane and transferred by wet transfer (Bio-Rad Laboratories AG, Fribourg, Switzerland). The membrane was coated in blocking buffer for an hour at room temperature, followed by primary antibodies overnight at 4°C, and then one hour in secondary antibodies at room temperature. Primary antibodies were as follows: anti-postsynaptic density protein 95 (PSD-95; mouse; 1:1000; Cat# ab2723; Abcam, Cambridge UK), anti-brain derived neurotrophic factor (BDNF; rabbit; 1:1000; Cat# ab108319; Abcam), anti-GluR2 & 3 (rabbit; 1:1000; Cat# AB1506; Sigma-Aldrich, St. Louis, Missouri, United States), anti-synapsin 1 (rabbit; 1:1000; Cat# ab1543p; Abcam), and anti- β -Tubulin (mouse; 1:10000; Cat# 86298; Cell Signaling Technology, Danvers, MA, USA) antibodies. These antibodies are involved in the regulation of synaptic transmission and plasticity. Secondary antibodies were as follows: horseradish peroxidase-conjugated affinity-pure goat anti-mouse IgG(H+L) (1:1000; Cat# SA00001-1; Proteintech, Wuhan, Hubei Province, China), and horseradish peroxidase-conjugated affinity-pure goat anti-rabbit IgG (H+L) (1:1000; Cat# SA00001-2; Proteintech). The protein bands were measured using an enhanced chemiluminescence detection kit (BeyoECL Moon, Cat# P0018FS, Beyotime Institute of Biotechnology, Haimen, Jiangsu Province, China) and exposed to DRAFT-FluorChem Q (Alpha Innotech Corporation, San Leandro, CA, USA). Signal intensities were quantified using ImageJ 1.46a (National Institutes of Health, Bethesda, MD, USA) and normalized to a reference protein (Tublin).

Immunoelectron microscopy

Rats were transcardially perfused under deep anesthesia at 21 days after MCAO. The hippocampal cornu ammonis 3 (CA3) region was quickly removed, cut into a $1 \times 1 \times 1 \text{ mm}^3$ size, placed into 2.5% glutaraldehyde in 0.1 μM phosphate buffer and fixed for 2 hours or longer. It was rinsed with 0.1 M phosphate 3 times, for 5 minutes each time. The tissues were fumigated in the carbonization chamber with osmium tetroxide for 0.5–2 hours, covered with 100% acetone twice, for 5 minutes each time, then a mixture of epoxy resin and 100% acetone. The tissues were shaken at room temperature for 15 minutes or at 1000 r/min for 5 minutes, then placed in an oven at 38°C for 2–3 hours. The permeate solution was removed as much as possible. Pure epoxy resin was placed in a 38°C oven for 1 hour, and then was embedded and labeled. After heating at 40°C for 1–2 hours, then 70°C overnight, the tissue was cut into 80-nm sections using an ultrathin slicer (Gao, 2015). For immunogold labeling, the vibratome grids were incubated with 50 mM glycine and 2.1% sodium perio-

date. The grids were then incubated for 24 to 48 hours at 4°C in droplets containing the primary antibody PSD-95 (mouse; 1:50; Cat# ab2723; Abcam), and GluA2/3 (rabbit; 1:50; Cat# AB1506; Sigma-Aldrich). After blocking with 1% bovine serum albumin for 20 minutes, the grids were then incubated for 2 hours with the secondary antibody. Secondary antibodies were as follows: Anti-Rabbit IgG (10 nm colloidal gold; 1:100; Cat# G7402; Sigma-Aldrich), and Anti-Mouse IgG (5 nm colloidal gold; 1:100; Cat# G7527; Sigma-Aldrich). After drying, 5% uranyl acetate and uranium citrate (or lead acetate) were used for staining, and then the grids were examined under a transmission electron microscope (80 kV; JEOL JEM-1230, Tokyo, Japan). A functional synapse was identified using the following criteria: a) contains PSD-95 (5 nm gold particles), b) exhibits well-defined membranes, clefts, and postsynaptic densities, c) contains at least two target gold particles within the postsynaptic area. The grids were measured with ImageJ software as described previously (Zhang et al., 2016). Particle density was calculated as the number of gold particles per linear micrometer ($\text{gold}/\mu\text{m}$); the distance between the center of each gold particle and the middle of the PSD was measured for synaptic location; the numbers of vesicles within 100 nm of the membrane was counted; and the size of these vesicles within 100 nm of the membrane of the presynaptic active zone (AZ) was measured with ImageJ software.

High-performance liquid chromatography

Rats were sacrificed under anesthesia at 21 days after MCAO for brain tissue preparation. The brain tissue was weighed on a balance pan, and 1.0 mg was added to 10 μL of 0.4 N perchloric acid solution. The solution was ultrasonically homogenized on ice for about 10–20 seconds five times, and the supernatant was collected after 10,000 r/min centrifugation for 10 minutes at 4°C. Levels of Asp, Glu, Asn, Gln, Gly, Tau, and GAMMA-amino butyric acid (GABA) were measured using a high-performance liquid chromatography system (Agilent Technologies, Santa Clara, CA, USA) as described previously (Smith and Sharp, 1994; Beverly et al., 2001). Briefly, the sample's supernatants were injected into an Eclipse XDB C18 column at 24°C. The separation flow rate was 0.8 mL/min. Phase A consisted of 0.1 M KH_2PO_4 , methanol, and tetrahydrofuran. Phase B was 90% methanol. A 13- μL sample and 7 μL of OPA reagent were mixed three times for the in-needle derivatization. After the above steps, the mixture of 20 μL was injected into the LC system for analysis. The total acquisition time was 20 minutes, then a step gradient was programmed, and the system could equilibrate during the derivatization and injection. The excitation wavelength was 340 nm, and the emission wavelength was 420 nm. Peaks and relative concentrations were determined by known standards. The data were collected and analyzed by ChemStation (Agilent Technologies).

Statistical analyses

All experimental data were analyzed using GraphPad Prism 7.0 (GraphPad Software Inc., San Diego, CA, USA) and SPSS

20.0 software (IBM Corporation, Armonk, NY, USA). The behavioral data were analyzed using a two-way analysis of variance with repeated measures and the Newman-Keuls multiple paired comparison for *post hoc* comparisons. The ratios of glutamate/glutamine and glutamate/GABA were compared between groups using one-way analysis of variance with equal variance followed by Tukey's multiple comparisons *post hoc* tests. GluR2/3 distribution was tested by the chi-square test. A value of $P < 0.05$ was considered statistically significant.

Results

mCIMT restores neurological function in MCAO rats

The experimental design is shown in **Figure 1A**. In the Catwalk gait analysis, the mean intensity of both right front limb and hind limb in the mCIMT group was higher at Day 21 compared with the MCAO group ($n = 6/\text{group}$, Front: $P = 0.00010$, Hind: $P = 0.00020$; **Figure 1B**). The adhesive removal test revealed that, 20 days after MCAO, the right front limb removal time in both MCAO groups was still significantly longer than that of the sham group rats. Rats in the MCAO and mCIMT groups displayed deficits to remove the tape. More importantly, a significant lower time in mCIMT compared to MCAO group was found at 20 days ($N = 6/\text{group}$, $P = 0.049$, **Figure 1C**), which indicates that the mCIMT group experienced an increase in the sensorimotor function; however, there was no significant between-group difference at 6, 9, or 15 days. The working memory performance in the Y maze (**Figure 1D**) revealed that the mCIMT and MCAO groups exhibited a significant lower score in the percentage of correct alternations at day 7 compared with sham group ($n = 6/\text{group}$, mCIMT: $P = 0.028$, MCAO: $P = 0.049$, **Figure 1D**). However, no significant difference was found in Y-maze test between the mCIMT and MCAO groups. For the entire experimental period, there were no significant differences in body weight between the mCIMT and MCAO groups (**Figure 1E**).

The effect of mCIMT on neurotransmitter receptor gene expression in the bilateral hippocampi after MCAO

To identify the role of the neurotransmitter receptor system in mCIMT after MCAO, we performed real-time quantitative PCR microarray on mRNA from 8 rats ($n = 4/\text{group}$ in MCAO and mCIMT groups) for 84 genes that were selected to represent neural transmitter receptors with differential samples in the bilateral hippocampi 21 days after MCAO (**Figure 2A**). The volcano plot illustrated that genes difference between MCAO group and mCIMT group in the left side (ischemic) hippocampus as well as in the right side (contralateral) hippocampus at 21-day MCAO (**Figure 2B** and **C**). *Gria3* was upregulated in the contralateral hippocampus in the mCIMT group compared to the MCAO group ($n = 4/\text{group}$; $P = 0.0041$; **Figure 2C**). Similarly, we found lower mRNA levels of the beta3-adrenergic receptor gene, *Adrb3*, and lower levels of Arginine Vasopressin Receptor 1A, *Avpr1a*, in mCIMT group compared to the MCAO group ($n = 4/\text{group}$; rat-*Avpr1a*, $P = 0.047$; rat-*Adrb3*, $P =$

0.049). In the ischemic side hippocampus, *Adra2a* was down-regulated ($n = 4/\text{group}$; $P = 0.036$) and *Gria3* tended to unregulated in mCIMT group compared to the MCAO group ($n = 4/\text{group}$; $P = 0.059$). All gene data are listed in **Table 2**.

mCIMT leads to an increase in immuno-labeled GluR2/3 expression in the CA3 region of the contralateral hippocampus

We compared GluR2/3 gold particle number and localization within the postsynaptic membrane in the CA3 region of the hippocampus between the three groups at 21 days after MCAO (**Figure 3A** and **B**). Double-label post-embedding immunoelectron microscopy was used to visualize GluR2/3 (10 nm colloidal gold particles) and PSD-95 (5 nm). We compared the sum of gold particles and localization patterns in the post-synaptic membrane ($n = 4/\text{group}$; 16 synapses/group). The results revealed that 73.74%, 63.64%, and 63.22% of GluR 2/3 immunogold particles in the mCIMT, MCAO, and sham groups were located within 240 nm of PSD-95 in the postsynaptic area (**Figure 3C**). The results of the statistical analysis are shown in **Figure 3D**. The total number of gold particles within 120–240 nm of PSD-95 was 42, 11, and 33 in the mCIMT, MCAO, and sham groups, respectively. Furthermore, the mCIMT group showed more profiles with a greater number of gold particles when compared with the MCAO group in the CA3 region of the hippocampus, after allocating the synapses into one of the following categories: one to three postsynaptic gold particles; four to six postsynaptic gold particles; seven to nine postsynaptic gold particles. The difference between mCIMT group and control group reached statistical significance ($n = 4/\text{group}$; chi-square test, $P = 0.0108$; **Figure 3D**).

The effect of mCIMT on GluR2/3 and BDNF expression in the contralateral hippocampus

At 21 days after MCAO, the tissue samples were harvested from the contralateral hippocampus of rats, and western blotting analysis was performed. GluR2/3 expression was higher in mCIMT group than in both the MCAO and sham groups ($n = 6/\text{group}$, $P = 0.0041$), and BDNF was higher in the mCIMT group than in the MCAO group ($n = 6/\text{group}$, $P = 0.026$). The levels of PSD-95 and synapsin I in the mCIMT group were similar to those in the MCAO group (**Figure 4A** and **B**).

The effect of mCIMT on SV in the ultrastructure of the CA3 region of the contralateral hippocampus

Under the electron microscope, the presynaptic AZ was seen to be an electron-dense area close to the membrane (**Figure 5A**). Vesicles within 100 nm of the AZ were widely studied, and SV populations are functionally homogeneous in this range. We compared vesicles in the pre-synaptic membrane ($n = 4/\text{group}$; 16 synapses/group). At 21 days after MCAO, there were no significant changes in SV size within 100 nm of the AZ among synapses of three group after between-group comparison (**Figure 5B**), and there were no significant between-group differences in the distribution of the vesicles within 100 nm of the AZ in the CA3 region (**Fig-**

ure 5C). Glutamate vesicle size, number, and distribution expression was unchanged in the contralateral hippocampus during the recovery phase in the mCIMT group (Figure 5).

mCIMT results in lower relative glutamate content in the contralateral hippocampus

At 21 days after MCAO, we collected the contralateral hippocampus and determined the content of the amino acid neurotransmitter using high-performance liquid chromatography. The ratio of glutamate/glutamine and the ratio of glutamate/GABA in the MCAO and mCIMT groups were significantly different after between-group comparison (mCIMT group: $n = 5$, MCAO group: $n = 5$, sham group: $n = 3$) (Glu/Gln: $P = 0.0296$, Glu/GABA: $P = 0.0034$), and the MCAO group had higher glutamate content in the contralateral hippocampus than the sham group ($P = 0.012$; Figure 6A). The content of Asp, Glu, Asn, Gln, Gly, Tau, and GABA in the contralesional hippocampus is shown in Figure 6B in each group.

Discussion

In this study, we demonstrated the neuroprotective effects of mCIMT, a novel intervention for affected limb training against cerebral ischemic injury in rats. This study clarified mCIMT improved the sensory and motor function of affected limb in rats with MCAO, but not cognitive function. Our results also suggest that mCIMT up-regulated the gene expression of Gria3 and the protein expression of GluR2/3 and BDNF in the contralateral hippocampus during the MCAO recovery phase. Moreover, GluR2/3 expression was upregulated within 240 nm to the postsynaptic density areas in the contralateral hippocampus of the mCIMT group. Here, the GluR process was investigated according to the immune colloidal gold co-labeling method, which provided strong evidence that mCIMT enhanced GluR2/3 expression in the postsynaptic membrane. In addition, our results indicated that mCIMT reversed the contralateral abnormal glutamate metabolism by high-performance liquid chromatography in the post-stroke recovery phase. To the best of our knowledge, the theoretical hypothesis proposed in this study verified that, mCIMT was strengthened in the recovery mechanism of stroke rehabilitation.

Currently, few studies have investigated the specific methods for mCIMT strategy. Among them, one study used forced arm, another variant of CIMT, following photothrombotic stroke, but no long-term improvements in motor function observed (Müller et al., 2008). In the present study, mCIMT was established for rat experiments, which had the following advantages. First, the unbearable constraint to the normal limb for social activities was temporary. Second, there was no need for animal anesthesia in mCIMT. Importantly, compared with a previous study, the mCIMT in our study was closer to that used in clinical practice, in that it considered the frequency, the amount, and the aerobic exercise type. mCIMT was initiated on the 7th day after stroke. Training time is a critical factor that determined the effects of rehabilitative training (Yagi et al., 2017), while

early training has been found to exacerbate brain damage (Li et al., 2017b). Based on the body weight measurements taken every other day, we can conclude that our daily 2-hour mCIMT introduced no stress in rats.

As far as we know, few comprehensive behavioral tests for its efficacy have been established. Rats exhibit subtle behavioral changes, which means that high-quality behavioral tests are required. In this experiment, two standardized tests were selected to assess the neurobehavioral performance indicative of motor and sensory neurological functions. In the adhesive removal test, the mCIMT group took less time to remove the adhesive using the affected limb than did the MCAO group, which indicates that mCIMT rats had a higher paw and mouth sensitivity, correct dexterity, and a better recovery of sensorimotor functional deficits. The behavioral results therefore confirmed the reliability of mCIMT. There was no significant difference between the mCIMT and MCAO groups in the Y-maze test. This could indicate that the molecular changes in mCIMT group were involved in functional recovery rather than a cognitive response to the constraint.

Two major populations of AMPAR complexes – those made up of GluR1 and GluR2, and those made up of GluR2 and GluR3. In addition, GluR2/3 subunits are stably tethered to the synapse. We found that the Gria3 gene was highly expressed in the contralateral hippocampus of the mCIMT group on the 21st day after MCAO. GluR2/3 subunits are stably tethered to the synapse (Wenthold et al., 1996), playing a critical role in generating depolarization (Isaac et al., 2007). Our immunogold labeling results demonstrated that GluR2/3 expression was upregulated within 240 nm to the postsynaptic density areas in the contralateral hippocampus of the mCIMT group. In this study, AMPAR were screened from the postsynaptic membrane of hippocampi according to the simultaneous co-labeling of PSD-95 and AMPAR. PSD-95 is located in the postsynaptic density, which is involved in anchoring synaptic proteins (Hunt et al., 1996; Sheng and Sala, 2001), and also acts as a non-silent AMPAR binding partner (Meyer et al., 2014). Furthermore, the immunogold labeling results at the protein level were verified by western blotting results. Previous studies showed that synapses become strengthened for a short time after an increase in AMPAR number (Takumi et al., 1999; Andrasfalvy and Magee, 2001). Nonetheless, it remains unclear whether stimulating neuronal excitability enhances motor performance after stroke. According to our results, modulating AMPAR signaling improved behavioral outcomes; this is similar to previous reports of the presence of a turning point from harm to benefit following stroke. Namely, the improved delivery of synaptic AMPAR starting 5 days after stroke should improve neural repair (Clarkson et al., 2011) and results in motor function recovery following brain injury (Abe et al., 2018). Glutamatergic signaling is strengthened via up-regulation of Ca²⁺/calmodulin-dependent protein kinase II, as well as its secondary and tertiary messengers, thereby resulting in upregulated cyclic adenosine monophosphate response element-binding protein (CREB) signaling, which

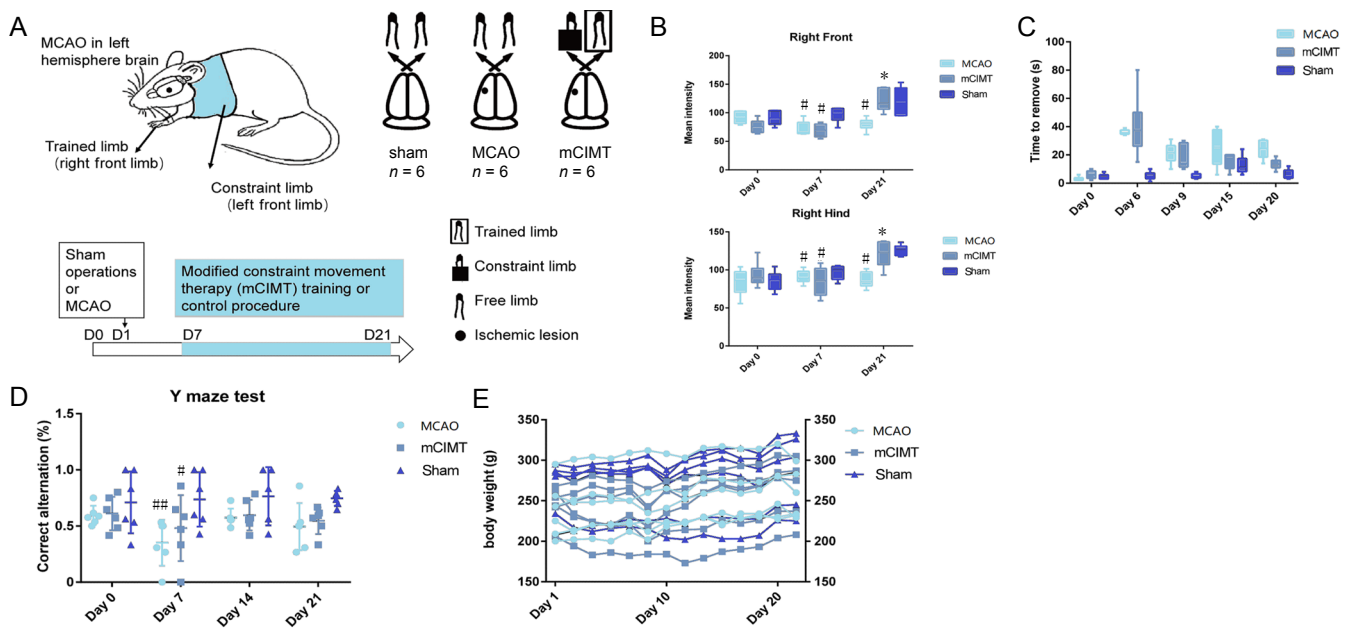


Figure 1 Effects of mCIMT on behavioral function before and after MCAO.

(A) The experimental design of behavioral tests for motor, sensory, and memory function. (B) Catwalk automated gait analysis ($n = 6/\text{group}$). (C) Adhesive removal performance. A longer time required to remove the adhesive tape on the right front paw indicates more severe sensory deficits ($n = 6/\text{group}$). (D) Y-maze test ($n = 6/\text{group}$). A lower ratio of collected alternations/maximum alternations indicates a more severe dysfunction of spatial working memory in the spontaneous alternation task. (E) Body weight. Bars represent group means (\pm SEM). The behavioral data were analyzed using two-way analysis of variance with repeated measures and Newman-Keuls multiple paired comparison for *post hoc* comparisons. # $P < 0.05$, ## $P < 0.01$, vs. sham group; * $P < 0.05$, vs. MCAO group. MCAO: Middle cerebral artery occlusion; mCIMT: modified constraint movement therapy; Right Front: right front paw; Right Hind: right hind paw.

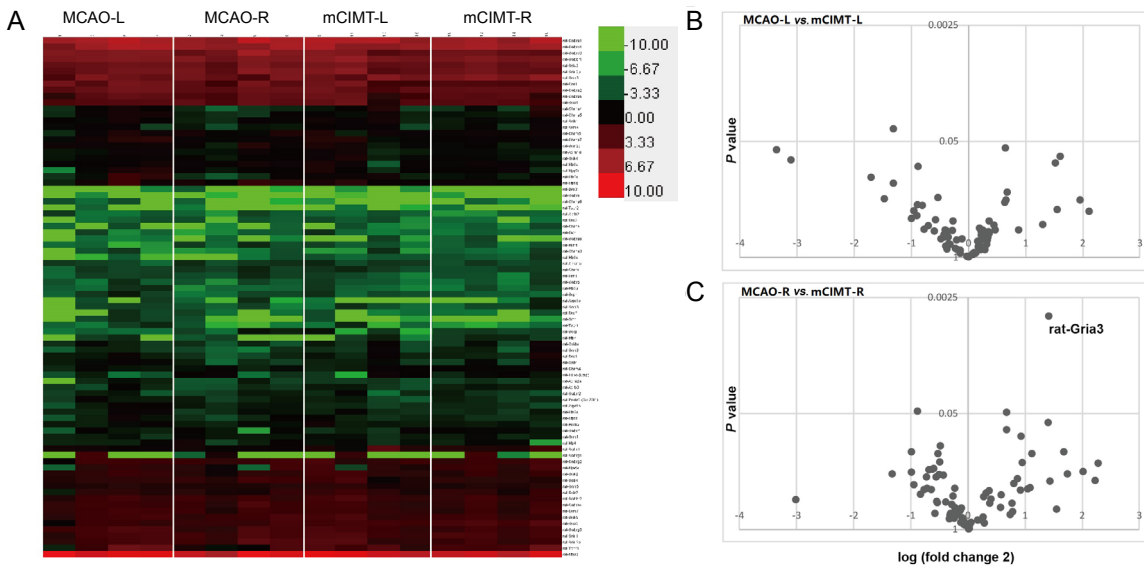


Figure 2 The mCIMT upregulated *Gria3* gene expression in the contralateral hippocampus after MCAO.

(A) Heat map showing changes in the expression of 84 neurotransmitter receptor genes in the hippocampus from the left side (ischemic) and the right side (contralateral) in the mCIMT and MCAO groups 3 weeks after MCAO ($n = 4/\text{group}$; color bars represent the Z-score range). Red and green shades represent a lower and higher relative expression, respectively. (B, C) A volcano plot for data of the 84 neurotransmitter receptor genes, which shows the difference in the hippocampus from the left side (ischemic; B) and the right side (contralateral; C) in the mCIMT and MCAO groups 3 weeks after MCAO ($n = 4/\text{group}$). MCAO: Middle cerebral artery occlusion; MCAO-L: the left region of MCAO group; MCAO-R: the right region of MCAO group; mCIMT: modified constraint movement therapy; mCIMT-L: the left region (ischemic) of mCIMT group; mCIMT-R: the right region (contralateral) of mCIMT group.

enhances motor recovery after stroke (Caracciolo et al., 2018).

We also found that the protein expression level of BDNF was higher in mCIMT group. Notably, glutamatergic neurotransmission is closely associated with the BDNF activity.

BDNF can be upregulated via Lyn-mitogen-activated protein kinase, the extracellular signal-regulated protein kinases 1/2, or the mammalian target of rapamycin pathway induced by the AMPAR-positive allosteric modulators (Hayashi et al., 1999; Clarkson et al., 2011; Fumagalli et al., 2012; Xie et

Table 1 mCIMT and MCAO group differences for 84 neurotransmitter receptor genes in the left side (ischemic) and the right side (contralateral) detected by microarray

Target name	MCAO-R/mCIMT-R	Log2	P-value	Target name	MCAO-L/mCIMT-L	Log2	P-value
rat-Gria3	0.375070565	-1.41476605	0.004062603	rat-Adra2a	2.494666202	1.318846789	0.036231163
rat-Avpr1a	1.844941517	0.883575085	0.046677791	rat-Gria3	0.64113361	-0.641303055	0.059364483
rat-Adrb3	0.625397299	-0.677155107	0.048840982	rat-Chrna6	10.29641193	3.364069773	0.062546425
rat-Gabrd	0.37781456	-1.404249793	0.063030842	rat-Htr1d	0.33000853	-1.599424779	0.073866737
rat-Chrm4	0.623690126	-0.681098676	0.075912557	rat-Avpr1b	8.628598182	3.109126196	0.080507692
rat-Grm3	0.523894916	-0.932650633	0.08987514	rat-Hrh4	0.348514781	-1.520708251	0.087154038
rat-Htr1a	1.402367975	0.487864956	0.115385573	rat-Sstr1	1.844345269	0.883108759	0.09513175
rat-Htr1b	1.983732285	0.98821734	0.133983405	rat-Drd5	3.251702934	1.701195463	0.126665484
rat-Tacr3	0.313384815	-1.673992821	0.134814363	rat-Avpr1a	2.484281288	1.312828535	0.148055895
rat-Htr7	0.460271569	-1.119442766	0.140957868	rat-Adra1a	0.623588877	-0.681332899	0.187098678
rat-Sstr4	1.438303842	0.524368478	0.141412371	rat-Gabrb3	1.452823905	0.538859846	0.212464828
rat-Gria1	1.407718374	0.493358739	0.174442547	rat-Sctr	2.774722442	1.472343464	0.220641442
rat-Npy5r	0.516343876	-0.953595899	0.176130705	rat-Tspo (Bzrp)	0.259030954	-1.948803588	0.225519234
rat-Grm8	0.205481936	-2.282916526	0.179169217	rat-Sstr2	0.63331079	-0.659014435	0.227660251
rat-Chrm1	1.510390016	0.594921133	0.207741161	rat-Chrm1	0.645834148	-0.630764371	0.242486472
rat-Grin2b	1.537647597	0.620724899	0.211692161	rat-Htr2a	1.854698264	0.891184497	0.257700383
rat-Grin2a	1.609515255	0.686626251	0.213736794	rat-Prokr2 (Grp73l1)	1.750354791	0.807647381	0.261823432
rat-Drd1	0.247654088	-2.013601658	0.223197729	rat-Gabrd	0.340459129	-1.554446477	0.29128136
rat-Hrh4	1.990522066	0.993146864	0.228226677	rat-Ntsr2	1.940386052	0.956343714	0.30081868
rat-Gabrb3	2.505016477	1.324820093	0.236389466	rat-Gcgr	0.232059574	-2.107432873	0.306760254
rat-Cckbr	0.298285095	-1.745236207	0.237388117	rat-Htr3a	1.87686293	0.908323292	0.340361563
rat-Adra1a	1.418453597	0.504318956	0.241470057	rat-Htr2c	1.99730696	0.998056074	0.366546511
rat-Grik4	1.352202326	0.435311034	0.246603264	rat-Chrna5	1.488256447	0.573623144	0.375484067
rat-Cnr1	1.647393242	0.720184975	0.256715216	rat-Gabrg3	1.207504215	0.272028225	0.387158001
rat-Adra1d	1.471489124	0.557276879	0.257876798	rat-Gabrr2	0.778038105	-0.36208728	0.388479605
rat-Htr3a	0.547300079	-0.86959603	0.268108497	rat-Gabra6	0.406941238	-1.297107609	0.43074933
rat-Chrna4	0.213118825	-2.23027006	0.283454683	rat-Chrm4	0.734333674	-0.445492335	0.433031087
rat-Sstr1	0.368611265	-1.439827935	0.285357885	rat-Grpr	1.628460525	0.703508748	0.439940692
rat-Grm4	0.574567851	-0.799450823	0.306680112	rat-Grm5	0.873098137	-0.195784271	0.471564081
rat-Adrb2	1.921513721	0.942243278	0.313472982	rat-Chrne	1.7191518	0.78169694	0.481064315
rat-Grm6	0.471894201	-1.083464651	0.339408131	rat-Grin2a	0.724063538	-0.465811793	0.489026854
rat-Gabra2	1.171132601	0.227904434	0.342702564	rat-Grik2	0.84249741	-0.247255844	0.489602943
rat-Grin2c	1.645147426	0.718216874	0.344633927	rat-Grm8	0.545665936	-0.873910111	0.490250225
rat-Chrna5	0.482966783	-1.050004128	0.351970712	rat-Cnr1	1.326992928	0.408160682	0.492790151
rat-Gcgr	1.704609895	0.769441612	0.354283749	rat-Gabra2	1.220692172	0.287699434	0.496608405
rat-Hrh1	1.558549373	0.640203859	0.357262533	rat-Hrh1	1.296748349	0.374898533	0.507797269
rat-Chrna3	0.529355487	-0.917691209	0.362097709	rat-Tacr3	1.515595786	0.599885033	0.509865336
rat-Sstr2	0.774750213	-0.368196849	0.368374487	rat-Gabrr1	0.818451238	-0.289031629	0.511828081
rat-Grik2	0.803561933	-0.315518873	0.392328998	rat-Gria2	0.858005462	-0.220941263	0.512703528
rat-Htr4	1.782554549	0.833946226	0.400295447	rat-Grin2b	0.78199263	-0.354773083	0.513231405
rat-Htr2c	0.667680704	-0.582769749	0.407123579	rat-Gabrr1	1.309162238	0.388643894	0.518840391
rat-Grm1	1.200738413	0.263921887	0.424328984	rat-Grm1	0.828554317	-0.271331816	0.52722888
rat-Gabrb1	0.82493381	-0.277649728	0.430275075	rat-Gria1	0.781453294	-0.355768446	0.542660453
rat-Gabrr1	0.758373466	-0.399019608	0.455571931	rat-Grm6	1.344903687	0.42750286	0.557287147
rat-Sctr	8.071007694	3.01274881	0.464245717	rat-Grin1	0.853935162	-0.227801562	0.568019206
rat-Drd2	1.462056701	0.547999263	0.482819944	rat-Sstr4	0.796600073	-0.328072484	0.584487729
rat-Htr2a	1.304460042	0.383452752	0.492860189	rat-Adrb2	1.342810555	0.425255783	0.588166755
rat-Ntsr2	1.448426784	0.53448676	0.501614619	rat-Chrna7	1.282855436	0.359358604	0.588692819
rat-Chrne	0.586463866	-0.769885872	0.507055746	rat-Grik4	0.79173003	-0.336919522	0.590882357
rat-Oxtr	0.76825007	-0.380352101	0.510157443	rat-Htr1f	1.394331535	0.479573637	0.619986423
rat-Gabra5	1.217817527	0.284297982	0.525463024	rat-Grm7	1.085121113	0.117856075	0.622005094
rat-Htr1d	0.670966471	-0.575687421	0.56225535	rat-Grm3	0.811706289	-0.300970303	0.625082964
rat-Gria2	1.172808313	0.229967235	0.56909543	rat-Drd2	0.795784982	-0.329549422	0.63417183
rat-Chrna7	1.081713303	0.113318179	0.577512357	rat-Htr4	0.859876451	-0.217798709	0.637662423
rat-Gabrg1	0.340188963	-1.555591758	0.591761448	rat-Grin2c	1.155846814	0.208950208	0.639229353
rat-Gabra4	1.166714556	0.22245164	0.602618849	rat-Grik5	0.892576178	-0.163952792	0.660995769
rat-Gabrr1	1.099244664	0.136512529	0.607844852	rat-Htr1b	1.273161713	0.348415678	0.700500759
rat-Hctr2	1.117327365	0.160051942	0.614015963	rat-Cckbr	0.799424702	-0.322965943	0.70909865
rat-Gabra6	0.581359675	-0.78249709	0.629339381	rat-Npy2r	1.252366872	0.324657251	0.714765985
rat-Tacr1	1.496323016	0.581421648	0.661787179	rat-Gabrg2	0.884887352	-0.176434286	0.735037642
rat-Gabrr2	1.23318248	0.302386298	0.662672788	rat-Tacr1	1.322327425	0.403079451	0.742241401
rat-Prokr2 (Grp73l1)	1.142571695	0.192284695	0.677100213	rat-Grik1	0.891055436	-0.166412904	0.753427209
rat-Avpr1b	0.598140941	-0.741442625	0.68324995	rat-Hctr2	0.863964174	-0.210956605	0.762820581
rat-Htr1f	1.239239791	0.309455374	0.693446473	rat-Adrb3	1.170454398	0.227068726	0.75947633
rat-Adra2a	0.832407666	-0.264637844	0.727238178	rat-Chrna3	1.29602864	0.3740976	0.805936565
rat-Grik5	1.070667343	0.098510304	0.738644104	rat-Gabrq	1.159594713	0.21362066	0.810506423
rat-Gabra1	1.179538895	0.238222992	0.740424952	rat-Oxtr	0.8185263	-0.288899323	0.815114372
rat-Drd5	1.250429712	0.322423965	0.757008698	rat-Gabrr2	0.862816211	-0.212874813	0.815268221
rat-Gabrq	0.841716165	-0.248594271	0.775876032	rat-Drd1	1.109975311	0.150527587	0.833341738

Table 1 Continued

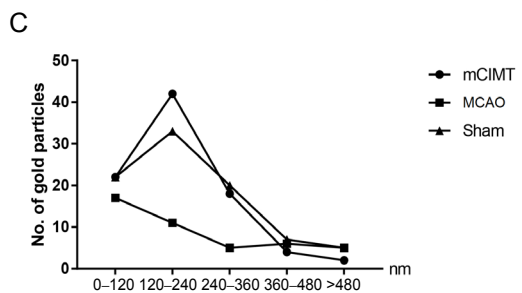
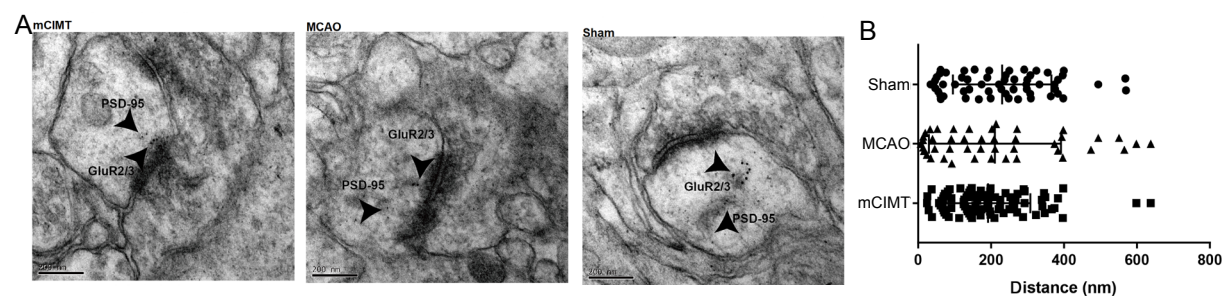
Target name	MCAO-R/mCIMT-R	Log2	P-value	Target name	MCAO-L/mCIMT-L	Log2	P-value
rat-Grik1	0.891357893	-0.165923284	0.778353912	rat-Grm4	0.936311268	-0.094939874	0.880485807
rat-Gabbr2	1.050947972	0.071691249	0.806094086	rat-Chrna4	0.911791852	-0.133223578	0.885661834
rat-Grpr	1.090711667	0.125269772	0.826778455	rat-Npy5r	0.924458726	-0.113319185	0.892674161
rat-Gabrg2	0.960045793	-0.058824873	0.830827196	rat-Htr1a	0.944059581-0.083050182	0.893529114	
rat-Chrna6	0.821557754	-0.283566098	0.846228636	rat-Htr7	1.109760047	0.15024777	0.894942075
rat-Grm7	1.047550297	0.067019515	0.865877004	rat-Chrm5	0.956388924	-0.064330672	0.920733964
rat-Grm5	0.979404866	-0.030022732	0.866846149	rat-Gabra5	0.954625942	-0.066992553	0.922483411
rat-Gabrg3	1.040357203	0.057078957	0.890017208	rat-Gabbr1	0.946342822	-0.079565186	0.927837119
rat-Npy2r	0.985523658	-0.021037591	0.963755915	rat-Adra1d	1.020598602	0.029415571	0.964238125
rat-Grin1	0.991488482	-0.012332081	0.967055923	rat-Gabra4	0.994501131	-0.007955083	0.976170743
rat-Tspo (Bzrp)	0.982744137	-0.025112243	0.974605667	rat-Gabra1	0.99538049	-0.006679985	0.987500831
rat-Chrm5	0.99265536	-0.010635179	0.980370634	rat-Brs3	1.395929071	0.481225638	#DIV/0!
rat-Brs3	#DIV/0!	#DIV/0!	#DIV/0!	rat-Gabre	7.655518005	2.9365	#DIV/0!
rat-Gabre	0.443037278	-1.1745	#DIV/0!	rat-Gabrg1	1.537407914	0.6205	#DIV/0!
rat-Tacr2	1.354653583	0.437923968	#DIV/0!	rat-Tacr2	4.017737152	2.006383183	#DIV/0!

There were 4 rats in each group. MCAO: Middle cerebral artery occlusion; MCAO-L: the left hippocampus of MCAO group; MCAO-R: the right hippocampus of MCAO group; mCIMT: modified constraint movement therapy; mCIMT-L: the left hippocampus (ischemic) of mCIMT group; mCIMT-R: the right hippocampus (contralateral) of mCIMT group.

Table 2 The relative expression of 84 neurotransmitter receptor genes in the hippocampus from the left side (ischemic) and the right side (contralateral) in mCIMT and MCAO groups 3 weeks after MCAO detected by real-time quantitative PCR

Target name	MCAO-L	MCAO-R	mCIMT-L	mCIMT-R	Target name	MCAO-L	MCAO-R	mCIMT-L	mCIMT-R
rat-Adra1a	0.000286	0.000439	0.000459	0.00031	rat-Gria3	0.008037	0.010715	0.012536	0.028567
rat-Adra1d	0.002149	0.001989	0.002105	0.001352	rat-Grik1	0.002328	0.001455	0.002612	0.001633
rat-Adra2a	0.000932	0.000426	0.000374	0.000512	rat-Grik2	0.008413	0.006337	0.009986	0.007887
rat-Adrb2	0.000187	0.000158	0.00014	8.23E-05	rat-Grik5	0.011111	0.011115	0.012448	0.010381
rat-Adrb3	0.000806	0.000365	0.000689	0.000583	rat-Grin1	0.012735	0.013912	0.014913	0.014031
rat-Avpr1a	0.001356	0.001022	0.000546	0.000554	rat-Grin2a	0.044086	0.066184	0.060886	0.04112
rat-Avpr1b	0.000319	0.000181	3.70E-05	0.000303	rat-Grin2b	0.01198	0.01628	0.01532	0.010588
rat-Brs3	4.63E-05	9.05E-05	3.32E-05	#DIV/0!	rat-Grin2c	0.003155	0.003023	0.00273	0.001837
rat-Cckbr	0.00081	0.000407	0.001013	0.001365	rat-Grm1	0.000881	0.001248	0.001063	0.001039
rat-Chrm1	0.000296	0.000467	0.000458	0.000309	rat-Grm3	0.042843	0.044488	0.052781	0.084918
rat-Chrm4	0.001132	0.001283	0.001541	0.002057	rat-Grm4	0.001744	0.000921	0.001863	0.001602
rat-Chrm5	0.002924	0.003111	0.003057	0.003134	rat-Grm5	0.005269	0.005241	0.006034	0.005352
rat-Chrna3	0.000212	9.44E-05	0.000163	0.000178	rat-Grm6	0.000311	0.000179	0.000231	0.00038
rat-Chrna4	0.002011	0.000476	0.002205	0.002236	rat-Grm7	0.011158	0.009639	0.010283	0.009202
rat-Chrna5	0.002792	0.001031	0.001876	0.002134	rat-Grm8	0.000533	0.000253	0.000976	0.001233
rat-Chrna6	0.000181	7.24E-05	1.75E-05	8.81E-05	rat-Grpr	0.000466	0.000181	0.000286	0.000166
rat-Chrna7	0.004605	0.00255	0.00359	0.002357	rat-Hctr2	0.001407	0.001124	0.001629	0.001006
rat-Chrne	0.00018	8.79E-05	0.000105	0.00015	rat-Hhr4	0.000274	0.000362	0.000211	0.000232
rat-Cnr1	0.045213	0.031471	0.034072	0.019104	rat-Htr4	6.48E-05	0.000336	0.000186	0.000169
rat-Drd1	0.001458	0.000408	0.001314	0.001646	rat-Htr1a	0.002387	0.002979	0.002528	0.002124
rat-Drd2	0.000151	0.000148	0.000189	0.000101	rat-Htr1b	0.00472	0.005437	0.003708	0.002741
rat-Drd5	0.000426	0.000163	0.000131	0.00013	rat-Htr1d	5.78E-05	0.000165	0.000175	0.000246
rat-Gabbr1	0.074288	0.069131	0.090767	0.06289	rat-Htr1f	0.001391	0.000845	0.000998	0.000682
rat-Gabbr2	0.009775	0.010235	0.012563	0.009739	rat-Htr2a	0.001657	0.000903	0.000894	0.000692
rat-Gabra1	0.291945	0.266873	0.2933	0.226252	rat-Htr2c	0.005165	0.000901	0.002586	0.001349
rat-Gabra2	0.040124	0.033759	0.03287	0.028826	rat-Htr3a	0.000342	0.000101	0.000182	0.000185
rat-Gabra4	0.009999	0.01118	0.010055	0.009583	rat-Htr4	0.001	0.001783	0.001163	0.001
rat-Gabra5	0.024714	0.02543	0.025889	0.020881	rat-Htr7	0.000492	0.00025	0.000443	0.000544
rat-Gabra6	7.54E-05	8.66E-05	0.000185	0.000149	rat-Npy2r	0.002901	0.001908	0.002317	0.001936
rat-Gabrb1	0.227919	0.170106	0.174095	0.206206	rat-Npy5r	0.006043	0.005629	0.006537	0.010902
rat-Gabrb3	0.080955	0.100094	0.055722	0.039957	rat-Ntsr2	1.975969	1.03099	1.018338	0.7118
rat-Gabrd	0.003013	0.00268	0.008848	0.007094	rat-Oxtr	0.000165	8.83E-05	0.000202	0.000115
rat-Gabre	4.14E-05	1.14E-05	5.41E-06	2.57E-05	rat-Prokr2 (Grp731)	0.001025	0.000774	0.000585	0.000677
rat-Gabrg1	0.013457	0.002099	0.008753	0.006169	rat-Sctr	0.00038	0.000122	0.000137	1.51E-05
rat-Gabrg2	0.0093	0.010254	0.01051	0.010681	rat-Sstr1	0.001597	0.000492	0.000866	0.001335
rat-Gabrg3	0.015475	0.011665	0.012815	0.011213	rat-Sstr2	0.005256	0.005925	0.0083	0.007648
rat-Gabrq	0.000254	0.000172	0.000219	0.000205	rat-Sstr4	0.006985	0.009472	0.008769	0.006586
rat-Gabbr1	0.000986	0.001221	0.001042	0.00161	rat-Tacr1	0.000301	6.81E-05	0.000227	4.55E-05
rat-Gabbr2	0.000657	0.000658	0.000761	0.000534	rat-Tacr2	0.000132	6.31E-05	3.28E-05	4.65E-05
rat-Gcgr	0.0001	0.000609	0.000433	0.000358	rat-Tacr3	0.023285	0.006633	0.015364	0.021164
rat-Gria1	0.02064	0.028042	0.026412	0.01992	rat-Tspo (Bzrp)	0.000367	0.001322	0.001417	0.001345
rat-Gria2	0.041524	0.04731	0.048395	0.040339					

There were 4 rats in each group. MCAO: Middle cerebral artery occlusion; MCAO-L: the left region of MCAO group; MCAO-R: the right region of MCAO group; mCIMT: modified constraint movement therapy; mCIMT-L: the left region (ischemic) of mCIMT group; mCIMT-R: the right region (contralateral) of mCIMT group.



No. of synapse contain GluR2/3	mCIMT(##)	MCAO	Sham
1-3 gold particles	3	10	6
4-6 gold particles	8	6	8
7-9 gold particles	5	0	2

Figure 3 Immunogold labeling showing postsynaptic localization of GluR2/3 in the contralateral hippocampal CA3 region.

(A) Double immunogold labeling of GluR2/3 (10 nm gold) and PSD-95 (5 nm gold). GluA2/3 gold particles and PSD-95 gold particles were co-localized on the postsynaptic membrane area. Scale bars: 200 nm. (B) Comparison of GluR2/3 gold particle number and localization at the postsynaptic membrane between the three groups. (C) Histogram showing the tangential distribution of immunogold of GluA2/3 on the postsynaptic region. The postsynaptic region was divided into 120-nm bins. (D) Table of the number of synapses containing different numbers of GluA2/3 particles. Data are expressed as the mean \pm SEM ($n = 4$ rats/group; number of synapses: $n = 16$ /group). # $P < 0.05$, vs. sham group; * $P < 0.05$, vs. MCAO group (chi-square test). CA3: Cornu ammonis 3; GluR: glutamate receptor; MCAO: middle cerebral artery occlusion; mCIMT: modified constraint movement therapy; PSD-95: postsynaptic density protein 95.

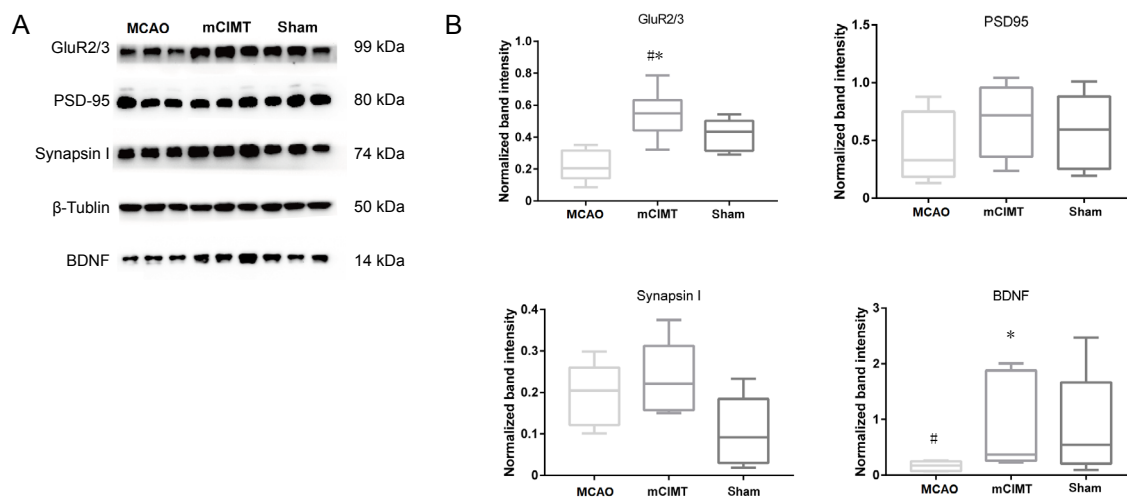
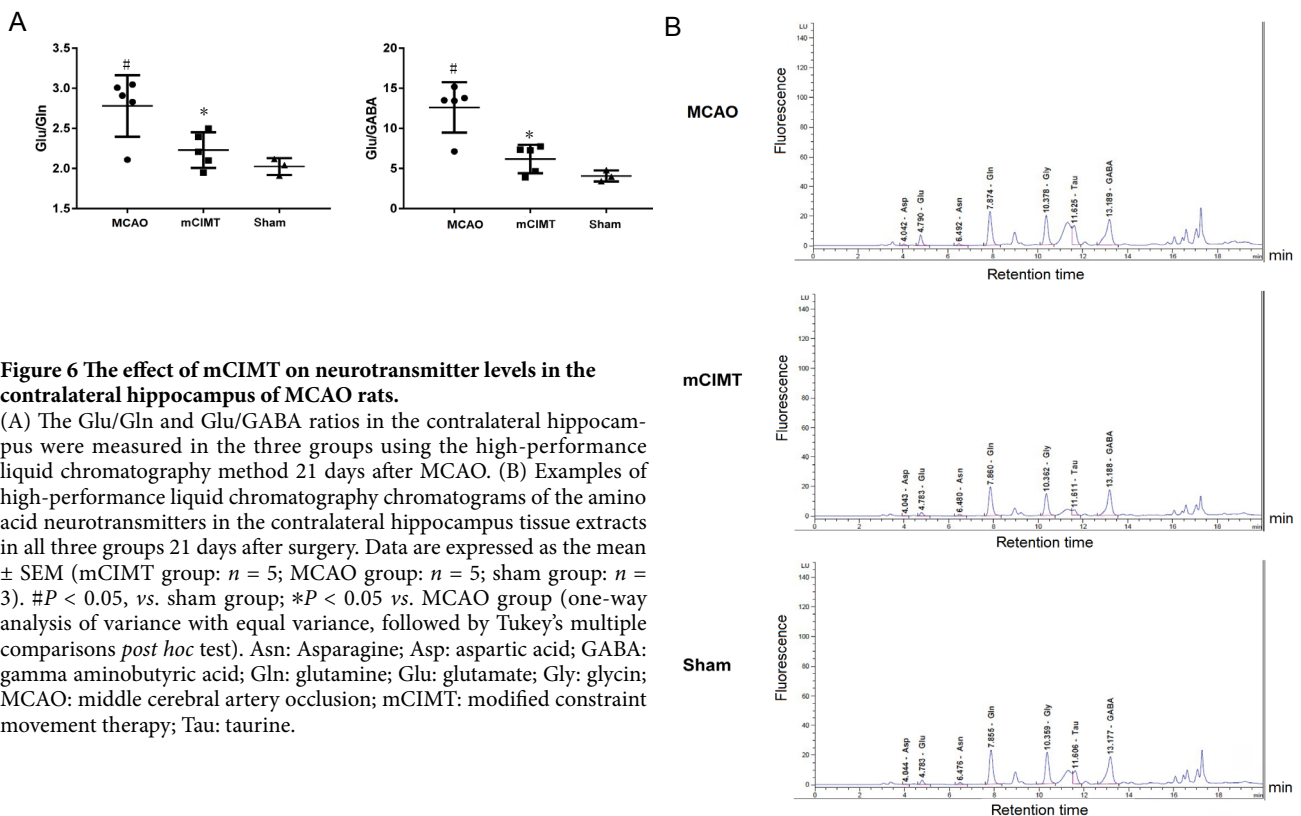
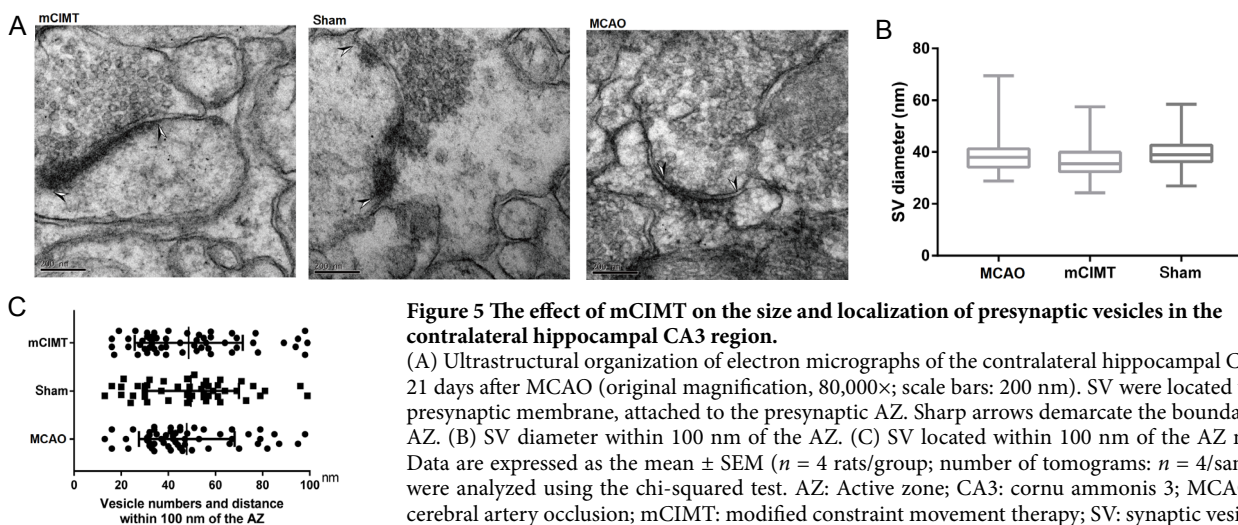


Figure 4 The mCIMT significantly upregulates GluR2/3 and BDNF in the contralateral hippocampus of MCAO rats. (A) Expression profiles of BDNF, PSD-95, Synapsin I, and GluR2/3 proteins in the contralateral hippocampus at the 21st day after MCAO. (B) Graphs indicate β -Tubulin-normalized protein levels of BDNF, PSD-95, Synapsin I, and GluR2/3. Data are expressed as the mean \pm SEM ($n = 6$ rats/group). # $P < 0.05$, vs. sham group; * $P < 0.05$, vs. MCAO group (one-way analysis of variance with equal variance, followed by Tukey's multiple comparisons *post hoc* test). BDNF: Brain-derived neurotrophic factor; GluR: glutamate receptor; MCAO: middle cerebral artery occlusion; mCIMT: modified constraint movement therapy; PSD-95: postsynaptic density protein 95.

al., 2013; Zhou et al., 2014). On the other hand, BDNF upregulates AMPAR expression and stimulates GluA1 protein synthesis in the brains of mammals (Du and Poo, 2004; Li and Wolf, 2011; Fado et al., 2015). Furthermore, AMPAR stimulation combined with local BDNF delivery is required to achieve maximal functional recovery following stroke in aged mice, which is achieved via the AKT-glycogen synthase kinase 3-CREB signaling pathway (Clarkson et al., 2015).

Increases in the AMPAR number and the amount of packaged glutamate released in response to action potentials

strengthens the synaptic signal. At glutamatergic nerve endings, SV attach to the presynaptic AZ, which gives rise to the readily-releasable pool (Südhof, 2013). SV within the range of 100 nm have been extensively investigated in the context of synaptic transmission, which is functionally similar with each other. According to our results, SV size and distribution were similar between the three groups in the contralateral hippocampus on the 21st day after MCAO. Additionally, our quantitative analysis of Synapsin I (which regulates the number of SV available for release) revealed no between-group



differences.

The glutamate-glutamine cycle and the reuptake rate of glutamate relies on glucose metabolism and ATP in the brain, as well as glial glutamate transporters; furthermore, glutamate dysfunction plays an essential role in the pathogenesis of ischemic brain injury (Neves et al., 2018). In our study, abnormal glutamate metabolism occurred in the MCAO group, but not in the mCIMT group, which might indicate that mCIMT balanced the glutamate-glutamine cycle. GABA is an inhibitory neurotransmitter. Glu/GABA was upregulated in the MCAO group compared with that in the sham and mCIMT groups, which is in line with reports of a significant reduction in GABA concentration after stroke (Kolasinski et al., 2019). Moreover, an increased glutamate

concentration was observed, which returned to normal levels in the serum by 48–72 hours after permanent middle cerebral artery occlusion (Leibowitz et al., 2012), which was consistent with our findings.

According to previous studies, CIMT improved functional recovery, enhanced glucose release in the contralateral hemisphere (Li et al., 2018), and upregulated hypoxia-inducible factor-1 α as well as vascular endothelial growth factor expression in rats with cerebral ischemia (Li et al., 2017a). Enhanced motor function and improved neural activity have also been reported in the contralateral hemisphere following intracerebral hemorrhage after motor skills training (Tama-koshi et al., 2014). In recent work, the contralesional side has been reported to play a significant role for at least a subset of

patients with stroke (Dodd et al., 2017), and patients with recent stroke commonly demonstrate increased M1 excitability in the contralesional hemisphere when moving the affected side for movements with the affected side (Chollet et al., 1991; Weiller et al., 1992; Butefisch et al., 2003; Murase et al., 2004; Butefisch et al., 2008; Tang et al., 2015). In both adult and pediatric CIMT studies, increased contralateral brain activities were observed using functional magnetic resonance imaging (Gauthier et al., 2008; Sterling et al., 2013). Altogether, these studies suggest that changes in contralateral neural network remodeling contributes to behavioral recovery following brain damage. Our finding of the upregulation of AMPAR in the contralesional hippocampus in the mCIMT group after stroke would enrich the content of mechanisms of mCIMT in recovering limb function, although the unregulated GluR2/3 and BDNF expression in the contralateral hippocampus remained to be further studied.

This study has some limitations that should be noted. Firstly, the lack of appropriate technical support meant that we could not link mCIMT alterations in the downstream pathway for AMPAR activation and the levels of other small molecules with their real-time changes in the brains of living animals. Secondly, we did not build a synaptic 3D image, and SV distance and size were not accurately calculated. Notably, one major breakthrough in ultrastructural analysis is to combine the resolution of vesicle placement (through synapse tomography fixed by high-pressure freezing) with immunogold labeling techniques (Imig et al., 2014), which will be examined in the future.

The present study demonstrated that mCIMT induced neurobehavioral improvements after MCAO. We observed upregulated GluR2/3 and BDNF expression in the mCIMT group, which could explain the mCIMT-induced neural repair. On the other hand, glutamate/glutamine and glutamate/GABA content in the contralateral hippocampus was higher in rats that had undergone MCAO than those in the mCIMT and sham groups. Thus, AMPAR activity and glutamate metabolism could represent a potential therapeutic target during the humans stroke recovery process. Altogether, these findings suggest that mCIMT plays a critical role in the regulation of glutamatergic synaptic plasticity and rescues sensory and motor decline after stroke.

Acknowledgments: The authors thank for Ms. Kong Yu from Institute of Neuroscience (ION), Chinese Academy of Sciences, Shanghai, China for her help with immunogold labeling and electron microscopy; Dr. Yuanyuan Ma at the State Key Laboratory of Medical Neurobiology of Fudan University, China for giving us professional support in the experiment of HPLC. Thanks Wcgen Biotech for their technical guidance on the microarray as well as and Mr. Hengji Zhang from Tongji University, China for his assistance in editing the manuscript.

Author contributions: Study design: YLB, BYG, DSX, YH, JH; experimental implementation: BYG, PLL, CL, LD, YH, JH; immunogold staining and analysis: JYH; molecular biology analysis: BYG, CL, PLL; manuscript writing: BYG; experiment supervision, statistical analysis supervision, and manuscript revising: YLB, DSX. All authors read and approved the final manuscript.

Conflicts of interest: The authors declare that there is no conflict of interests.

Financial support: The study was supported by the National Natural Science Foundation of China, No. 81871841 (to YLB) and No. 81772453 (to DSX). The funding bodies played no role in the study design, in the collection, analysis and interpretation of data, in the writing of the paper, or in the decision to submit the paper for publication.

Institutional review board statement: This study was approved by the Institutional Animal Care and Use Committee of Fudan University, China (approval No. 201802173S) on March 3, 2018.

Copyright license agreement: The Copyright License Agreement has been signed by all authors before publication.

Data sharing statement: Datasets analyzed during the current study are available from the corresponding author on reasonable request.

Plagiarism check: Checked twice by iThenticate.

Peer review: Externally peer reviewed.

Open access statement: This is an open access journal, and articles are distributed under the terms of the Creative Commons Attribution-Non-Commercial-ShareAlike 4.0 License, which allows others to remix, tweak, and build upon the work non-commercially, as long as appropriate credit is given and the new creations are licensed under the identical terms.

Open peer reviewer: Saman Sargolzaei, University of California Los Angeles, USA.

Additional files:

Additional Table 1: Rat neurotransmitter receptor genes in the rat neurotransmitter receptor PCR array

Additional file 1: Open peer review report 1.

References

- Abe H, Jitsuki S, Nakajima W, Murata Y, Jitsuki-Takahashi A, Katsuno Y, Tada H, Sano A, Suyama K, Mochizuki N, Komori T, Masuyama H, Okuda T, Goshima Y, Higo N, Takahashi T (2018) CRMP2-binding compound, edonepic maleate, accelerates motor function recovery from brain damage. *Science* 360:50-57.
- Andrasfalvy BK, Magee JC (2001) Distance-dependent increase in AMPA receptor number in the dendrites of adult hippocampal CA1 pyramidal neurons. *J Neurosci* 21:9151-9159.
- Baldwin CR, Harry AJ, Power LJ, Pope KL, Harding KE (2018) Modified constraint-induced movement therapy is a feasible and potentially useful addition to the community rehabilitation tool kit after stroke: a pilot randomised control trial. *Aust Occup Ther J* 65:503-511.
- Bang DH, Shin WS, Choi HS (2018) Effects of modified constraint-induced movement therapy with trunk restraint in early stroke patients: A single-blinded, randomized, controlled, pilot trial. *NeuroRehabilitation* 42:29-35.
- Bast T, Feldon J (2003) Hippocampal modulation of sensorimotor processes. *Prog Neurobiol* 70:319-345.
- Baumgartner P, El Amki M, Bracko O, Luft AR, Wegener S (2018) Sensorimotor stroke alters hippocampo-thalamic network activity. *Sci Rep* 8:15770.
- Beverly JL, De Vries MG, Bouman SD, Arseneau LM (2001) Noradrenergic and GABAergic systems in the medial hypothalamus are activated during hypoglycemia. *Am J Physiol Regul Integr Comp Physiol* 280:R563-569.
- Bouet V, Boulouard M, Toutain J, Divoux D, Bernaudin M, Schumann-Bard P, Freret T (2009) The adhesive removal test: a sensitive method to assess sensorimotor deficits in mice. *Nat Protoc* 4:1560-1564.
- Butefisch CM, Netz J, Wessling M, Seitz RJ, Homberg V (2003) Remote changes in cortical excitability after stroke. *Brain* 126:470-481.
- Butefisch CM, Wessling M, Netz J, Seitz RJ, Homberg V (2008) Relationship between interhemispheric inhibition and motor cortex excitability in subacute stroke patients. *Neurorehabil Neural Repair* 22:4-21.
- Caracciolo L, Marosi M, Mazzitelli J, Latifi S, Sano Y, Galvan L, Kawaguchi R, Holley S, Levine MS, Coppola G, Portera-Cailliau C, Silva AJ, Carmichael ST (2018) CREB controls cortical circuit plasticity and functional recovery after stroke. *Nat Commun* 9:2250.
- Chen X, Wang K (2016) The fate of medications evaluated for ischemic stroke pharmacotherapy over the period 1995-2015. *Acta Pharm Sin B* 6:522-530.
- Chollet F, DiPiero V, Wise RJ, Brooks DJ, Dolan RJ, Frackowiak RS (1991) The functional anatomy of motor recovery after stroke in humans: a study with positron emission tomography. *Ann Neurol* 29:63-71.
- Clarkson AN, Parker K, Nilsson M, Walker FR, Gowing EK (2015) Combined amphetamine and BDNF treatments enhance poststroke functional recovery in aged mice via AKT-CREB signaling. *J Cereb Blood Flow Metab* 35:1272-1279.
- Clarkson AN, Overman JJ, Zhong S, Mueller R, Lynch G, Carmichael ST (2011) AMPA receptor-induced local brain-derived neurotrophic factor signaling mediates motor recovery after stroke. *J Neurosci* 31:3766-3775.
- Coleman ER, Moudgal R, Lang K, Hyacinth HI, Awosika OO, Kissela BM, Feng W (2017) Early rehabilitation after stroke: a narrative review. *Curr Atheroscler Rep* 19:59.
- Dietrich MO, Andrews ZB, Horvath TL (2008) Exercise-induced synaptogenesis in the hippocampus is dependent on UCP2-regulated mitochondrial adaptation. *J Neurosci* 28:10766-10771.

- Dodd KC, Nair VA, Prabhakaran V (2017) Role of the contralesional vs. ipsilesional hemisphere in stroke recovery. *Front Hum Neurosci* 11:469.
- Du JL, Poo MM (2004) Rapid BDNF-induced retrograde synaptic modification in a developing retinotectal system. *Nature* 429:878-883.
- Fado R, Soto D, Minano-Molina AJ, Pozo M, Carrasco P, Yefimenko N, Rodriguez-Alvarez J, Casals N (2015) Novel regulation of the synthesis of alpha-amino-3-hydroxy-5-methyl-4-isoxazolepropionic acid (AMPA) receptor subunit GluA1 by carnitine palmitoyltransferase 1C (CPT1C) in the hippocampus. *J Biol Chem* 290:25548-25560.
- Feigin VL, Roth GA, Naghavi M, Parmar P, Krishnamurthi R, Chugh S, Mensah GA, Norrving B, Shieue I, Ng M, Estep K, Cercy K, Murray CJL, Forouzanfar MH (2016) Global burden of stroke and risk factors in 188 countries, during 1990-2013: a systematic analysis for the Global Burden of Disease Study 2013. *Lancet Neurol* 15:913-924.
- Fumagalli F, Calabrese F, Luoni A, Shahid M, Racagni G, Riva MA (2012) The AMPA receptor potentiator Org 26576 modulates stress-induced transcription of BDNF isoforms in rat hippocampus. *Pharmacol Res* 65:176-181.
- Gao HJ (2015) Bioelectron microscope sample carbonization method. China patent: No.201410183132.2.
- Gauthier LV, Taub E, Perkins C, Ortman M, Mark VW, Uswatte G (2008) Remodeling the brain: plastic structural brain changes produced by different motor therapies after stroke. *Stroke* 39:1520-1525.
- Hayashi M, Mitsunaga F, Ohira K, Shimizu K, Yamashita A (1999) Development of full-length Trk B-immunoreactive structures in the hippocampal formation of the macaque monkey. *Anat Embryol (Berl)* 199:529-537.
- Hu J, Li C, Hua Y, Zhang B, Gao BY, Liu PL, Sun LM, Lu RR, Wang YY, Bai YL (2019) Constrained-induced movement therapy promotes motor function recovery by enhancing the remodeling of ipsilesional corticospinal tract in rats after stroke. *Brain Res* 1708:27-35.
- Hunt CA, Schenker LJ, Kennedy MB (1996) PSD-95 is associated with the postsynaptic density and not with the presynaptic membrane at forebrain synapses. *J Neurosci* 16:1380-1388.
- Imig C, Min SW, Krinner S, Arancillo M, Rosenmund C, Südhof TC, Rhee J, Brose N, Cooper BH (2014) The morphological and molecular nature of synaptic vesicle priming at presynaptic active zones. *Neuron* 84:416-431.
- Isaac JT, Ashby MC, McBain CJ (2007) The role of the GluR2 subunit in AMPA receptor function and synaptic plasticity. *Neuron* 54:859-871.
- Kerr MSD, Sacré P, Kahn K, Park HJ, Johnson M, Lee J, Thompson S, Bulacio J, Jones J, González-Martínez J, Liégeois-Chauvel C, Sarma SV, Gale JT (2017) The role of associative cortices and hippocampus during movement perturbations. *Front Neural Circuits* 11:26.
- Kolasinski J, Hinson EL, Divanbeighi Zand AP, Rizov A, Emir UE, Stagg CJ (2019) The dynamics of cortical GABA in human motor learning. *J Physiol* 597:271-282.
- Kraeuter AK, Guest PC, Sarnyai Z (2019) The Y-maze for assessment of spatial working and reference memory in mice. *Methods Mol Biol* 1916:105-111.
- Kwakkel G, Veerbeek JM, van Wegen EE, Wolf SL (2015) Constraint-induced movement therapy after stroke. *Lancet Neurol* 14:224-234.
- Langhorne P, O'Donnell MJ, Chin SL, Zhang H, Xavier D, Avezum A, Mathur N, Turner M, MacLeod MJ, Lopez-Jaramillo P, Damasceno A, Hankey GJ, Dans AL, Elsayed A, Mondo C, Wasay M, Czlonkowska A, Weimar C, Yusufali AH, Hussain FA, et al. (2018) Practice patterns and outcomes after stroke across countries at different economic levels (INTERSTROKE): an international observational study. *Lancet* 391:2019-2027.
- Leibowitz A, Boyko M, Shapira Y, Zlotnik A (2012) Blood glutamate scavenging: insight into neuroprotection. *Int J Mol Sci* 13:10041-10066.
- Li C, Zhang B, Zhu Y, Li Y, Liu P, Gao B, Tian S, Du L, Bai Y (2017a) Post-stroke constraint-induced movement therapy increases functional recovery, angiogenesis, and neurogenesis with enhanced expression of HIF-1alpha and VEGF. *Curr Neurovasc Res* 14:368-377.
- Li F, Geng X, Khan H, Pandy JT Jr, Peng C, Li X, Rafols JA, Ding Y (2017b) Exacerbation of brain injury by post-stroke exercise is contingent upon exercise initiation timing. *Front Cell Neurosci* 11:311.
- Li X, Wolf ME (2011) Brain-derived neurotrophic factor rapidly increases AMPA receptor surface expression in rat nucleus accumbens. *Eur J Neurosci* 34:190-198.
- Li YY, Zhang B, Yu KW, Li C, Xie HY, Bao WQ, Kong YY, Jiao FY, Guan YH, Bai YL (2018) Effects of constraint-induced movement therapy on brain glucose metabolism in a rat model of cerebral ischemia: a micro PET/CT study. *Int J Neurosci* 128:736-745.
- Liang D, He XB, Wang Z, Li C, Gao BY, Wu JF, Bai YL (2018) Remote limb ischemic postconditioning promotes motor function recovery in a rat model of ischemic stroke via the up-regulation of endogenous tissue kallikrein. *CNS Neurosci Ther* 24:519-527.
- Liu XH, Bi HY, Cao J, Ren S, Yue SW (2019) Early constraint-induced movement therapy affects behavior and neuronal plasticity in ischemia-injured rat brains. *Neural Regen Res* 14:775-782.
- Longa EZ, Weinstein PR, Carlson S, Cummins R (1989) Reversible middle cerebral artery occlusion without craniectomy in rats. *Stroke* 20:84-91.
- Meyer D, Bonhoeffer T, Scheuss V (2014) Balance and stability of synaptic structures during synaptic plasticity. *Neuron* 82:430-443.
- Müller HD, Hanumanthiah KM, Diederich K, Schwab S, Schäbitz WR, Sommer C (2008) Brain-derived neurotrophic factor but not forced arm use improves long-term outcome after phot thrombotic stroke and transiently upregulates binding densities of excitatory glutamate receptors in the rat brain. *Stroke* 39:1012-1021.
- Murase N, Duque J, Mazzocchio R, Cohen LG (2004) Influence of interhemispheric interactions on motor function in chronic stroke. *Ann Neurol* 55:400-409.
- Neves JD, Vizuete AF, Nicola F, Da Re C, Rodrigues AF, Schmitz F, Mestriner RG, Aristimounha D, Wyse ATS, Netto CA (2018) Glial glutamate transporters expression, glutamate uptake, and oxidative stress in an experimental rat model of intracerebral hemorrhage. *Neurochem Int* 116:13-21.
- Nie J, Yang X (2017) Modulation of synaptic plasticity by exercise training as a basis for ischemic stroke rehabilitation. *Cell Mol Neurobiol* 37:5-16.
- Park J, Lee N, Cho Y, Yang Y (2015) Modified constraint-induced movement therapy for clients with chronic stroke: interrupted time series (ITS) design. *J Phys Ther Sci* 27:963-966.
- Qu HL, Zhao M, Zhao SS, Xiao T, Song CG, Cao YP, Jolkkonen J, Zhao CS (2015) Forced limb-use enhanced neurogenesis and behavioral recovery after stroke in the aged rats. *Neuroscience* 286:316-324.
- Sandvig I, Augestad IL, Haberg AK, Sandvig A (2018) Neuroplasticity in stroke recovery. The role of microglia in engaging and modifying synapses and networks. *Eur J Neurosci* 47:1414-1428.
- Sheng M, Sala C (2001) PDZ domains and the organization of supramolecular complexes. *Annu Rev Neurosci* 24:1-29.
- Smith S, Sharp T (1994) Measurement of GABA in rat brain microdialysates using o-phthalaldehyde-sulphite derivatization and high-performance liquid chromatography with electrochemical detection. *J Chromatogr* 652:228-233.
- Sterling C, Taub E, Davis D, Rickards T, Gauthier LV, Griffin A, Uswatte G (2013) Structural neuroplastic change after constraint-induced movement therapy in children with cerebral palsy. *Pediatrics* 131:e1664-1669.
- Stranahan AM, Khalil D, Gould E (2007) Running induces widespread structural alterations in the hippocampus and entorhinal cortex. *Hippocampus* 17:1017-1022.
- Südhof TC (2013) Neurotransmitter release: the last millisecond in the life of a synaptic vesicle. *Neuron* 80:675-690.
- Takemoto K, Iwanari H, Tada H, Suyama K, Sano A, Nagai T, Hamakubo T, Takahashi T (2017) Optical inactivation of synaptic AMPA receptors erases fear memory. *Nat Biotechnol* 35:38-47.
- Takumi Y, Ramirez-Leon V, Laake P, Rinkev E, Ottersen OP (1999) Different modes of expression of AMPA and NMDA receptors in hippocampal synapses. *Nat Neurosci* 2:618-624.
- Tamakoshi K, Ishida K, Kawanaka K, Takamatsu Y, Tamaki H (2017) Motor skills training enhances alpha-amino-3-hydroxy-5-methyl-4-isoxazolepropionic acid receptor subunit mRNA expression in the ipsilateral sensorimotor cortex and striatum of rats following intracerebral hemorrhage. *J Stroke Cerebrovasc Dis* 26:2232-2239.
- Tamakoshi K, Ishida A, Takamatsu Y, Hamakawa M, Nakashima H, Shimada H, Ishida K (2014) Motor skills training promotes motor functional recovery and induces synaptogenesis in the motor cortex and striatum after intracerebral hemorrhage in rats. *Behav Brain Res* 260:34-43.
- Tang Q, Li G, Liu T, Wang A, Feng S, Liao X, Jin Y, Guo Z, He B, McClure MA, Xing G, Mu Q (2015) Modulation of interhemispheric activation balance in motor-related areas of stroke patients with motor recovery: Systematic review and meta-analysis of fMRI studies. *Neurosci Biobehav Rev* 57:392-400.
- van Praag H, Christie BR, Sejnowski TJ, Gage FH (1999) Running enhances neurogenesis, learning, and long-term potentiation in mice. *Proc Natl Acad Sci U S A* 96:13427-13431.
- Vandenberg RJ, Ryan RM (2013) Mechanisms of glutamate transport. *Physiol Rev* 93:1621-1657.
- Weiller C, Chollet F, Friston KJ, Wise RJ, Frackowiak RS (1992) Functional reorganization of the brain in recovery from striatocapsular infarction in man. *Ann Neurol* 31:463-472.
- Wentholt RJ, Petralia RS, Blahos J, II, Niedzielski AS (1996) Evidence for multiple AMPA receptor complexes in hippocampal CA1/CA2 neurons. *J Neurosci* 16:1982-1989.
- Xie Y, Huang X, Hu SY, Zhang YJ, Wang Y, Qiu XJ, Ren P, Fan R, Zhang CH, Xie WB, Ji H, He J, Chen X, Xie L, Liu ZQ, Zhou HH (2013) The involvement of AMPA-ERK1/2-BDNF pathway in the mechanism of new antidepressant action of prokinetic meranzin hydrate. *Amino Acids* 44:413-422.
- Yagi M, Yasunaga H, Matsui H, Morita K, Fushimi K, Fujimoto M, Koyama T, Fujitani J (2017) Impact of rehabilitation on outcomes in patients with ischemic stroke: a nationwide retrospective cohort study in Japan. *Stroke* 48:740-746.
- Yau SY, Li A, Hoo RL, Ching YP, Christie BR, Lee TM, Xu A, So KF (2014) Physical exercise-induced hippocampal neurogenesis and antidepressant effects are mediated by the adipocyte hormone adiponectin. *Proc Natl Acad Sci U S A* 111:15810-15815.
- Yau SY, Lau BW, Tong JB, Wong R, Ching YP, Qiu G, Tang SW, Lee TM, So KF (2011) Hippocampal neurogenesis and dendritic plasticity support running-improved spatial learning and depression-like behaviour in stressed rats. *PLoS One* 6:e24263.
- Zhai ZY, Feng J (2019) Constraint-induced movement therapy enhances angiogenesis and neurogenesis after cerebral ischemia/reperfusion. *Neural Regen Res* 14:1743-1754.
- Zhang J, Petralia RS, Wang YX, Diamond JS (2016) High-resolution quantitative immunogold analysis of membrane receptors at retinal ribbon synapses. *J Vis Exp*:53547.
- Zhao S, Zhao M, Xiao T, Jolkkonen J, Zhao C (2013) Constraint-induced movement therapy overcomes the intrinsic axonal growth-inhibitory signals in stroke rats. *Stroke* 44:1698-1705.
- Zhou W, Wang N, Yang C, Li XM, Zhou ZQ, Yang JJ (2014) Ketamine-induced antidepressant effects are associated with AMPA receptors-mediated upregulation of mTOR and BDNF in rat hippocampus and prefrontal cortex. *Eur Psychiatry* 29:419-423.

Additional Table 1 Rat neurotransmitter receptor genes in the rat neurotransmitter receptor PCR array

Neurotransmitter receptor	Gene
Dopaminergic receptors	<i>Drd1a, Drd2, Drd5</i>
GABAergic receptors	
GABA _A	<i>Gabra1, Gabra2, Gabra4, Gabra5, Gabra6, Gabrb1, Gabrb3, Gabrd, Gabre, Gabrg1, Gabrg2, Gabrg3, Gabrq</i>
GABA _B	<i>Gabbr1, Gabbr2</i>
GABA _C	<i>Gabrr1, Gabrr2</i>
Glutamate receptors	
AMPA receptors	<i>Gria1, Gria2, Gria3</i>
Kainate receptors	<i>Grik1, Grik2, Grik4, Grik5</i>
NMDA receptors	<i>Grin1, Grin2a, Grin2b, Grin2c</i>
Metabotropic receptors	<i>Grm1, Grm3, Grm4, Grm5, Grm6, Grm7, Grm8</i>
Serotonin receptors	<i>Htr1a, Htr1b, Htr1d, Htr1f, Htr2a, Htr2b, Htr2c, Htr3a, Htr4, Htr7</i>
Other neurotransmitter receptors	
Vasopressin receptor	<i>Avpr1a, Avpr1b</i>
Histamine receptor	<i>Hrh1, Hrh4</i>
Neuropeptide Y	<i>Npy2r, Npy5r</i>
Somatostatin	<i>Sstr1, Sstr2, Sstr4</i>
Substance P (Neurokinin) receptor	<i>Tacr1, Tacr2, Tacr3</i>
Other receptors	<i>Brs3, Cckbr, Cnr1, Gcgr, Grpr, Hcrtr2, Ntsr2, Oxt, Prokr2 (Grp73l1), Tspo (Bzrp)</i>

AMPA: α -Amino-3-hydroxy-5-methyl-4-isoxazole-propionic acid; GABA: γ -aminobutyric acid; NMDA: N-methyl-D-aspartic acid.